

Dielectric function, screening, and plasmons of graphene in the presence of spin-orbit interactionsAndreas Scholz,^{1,*} Tobias Stauber,² and John Schliemann¹¹*Institute for Theoretical Physics, University of Regensburg, D-93040 Regensburg, Germany*²*Departamento de Física de la Materia Condensada and Instituto Nicolas Cabrera, Universidad Autónoma de Madrid, E-28049 Madrid, Spain*

(Received 21 June 2012; revised manuscript received 4 September 2012; published 21 November 2012)

We study the dielectric properties of graphene in the presence of Rashba and intrinsic spin-orbit interactions in their most general form, i.e., for arbitrary frequency, wave vector, doping, and spin-orbit coupling (SOC) parameters. The main result consists in the derivation of closed analytical expressions for the imaginary as well as for the real part of the polarization function. Several limiting cases, e.g., the case of purely Rashba or purely intrinsic SOC, and the case of equally large Rashba and intrinsic coupling parameters are discussed. In the static limit the asymptotic behavior of the screened potential due to charged impurities is derived. In the opposite limit ($q = 0$, $\omega \rightarrow 0$), an analytical expression for the plasmon dispersion is obtained and afterwards compared to the numerical result. Our result can also be applied to related systems such as bilayer graphene or topological insulators.

DOI: [10.1103/PhysRevB.86.195424](https://doi.org/10.1103/PhysRevB.86.195424)

PACS number(s): 77.22.Ch, 71.45.Gm, 81.05.ue

I. INTRODUCTION

It is now well established that at low energies the charge carriers in graphene are described by a Dirac-like equation for massless particles.^{1,2} While standard graphene, i.e., without any spin-orbit interactions (SOIs), does not exhibit a band gap, a gap opens up in the spectrum if one includes purely intrinsic spin-orbit interactions.³ The corresponding energy dispersion resembles that of a massive relativistic particle with a rest energy which is proportional to the spin-orbit coupling parameter (SOC). Including SOIs of the Rashba type, e.g., by applying an external electric field, lifts the spin degeneracy. Depending on the ratio of the intrinsic and the Rashba parameters a gap can occur in the spectrum or not.

Many theoretical studies on the dielectric function of various systems have been made in the last years. Besides semiconductor two-dimensional electron gases⁴⁻⁶ and hole gas systems,⁷ large investigations have been made in graphene. Starting from the simplest possible graphene model within the Dirac-cone approximation,⁸⁻¹⁰ more and more extensions have been included. These extensions range from numerical^{11,12} and analytical¹³ tight-binding studies and the inclusion of a finite band gap¹⁴⁻¹⁶ to double- and multilayer graphene samples,¹⁷⁻²² graphene antidot lattices,²³ and graphene under a circularly polarized ac electric field.²⁴

In this work we study the dielectric properties of graphene including both the Rashba and the intrinsic spin-orbit coupling. While the case of purely intrinsic interactions is well understood,¹⁴⁻¹⁶ the dielectric function for the general case, where both types of SOIs are present, is unknown. Other previous studies have investigated the effect of SOI on magnetotransport²⁵ and the optical conductivity.^{26,27}

Our study is motivated by recent experimental and theoretical works demonstrating that the SOC parameters can significantly be enlarged by choosing proper adatoms²⁸⁻³⁰ or a suitable environment.³¹⁻³³

Information that can be extracted from the dielectric function range from the screening between charged particles to the collective charge excitations formed due to the long-ranged Coulomb interaction. Knowledge of the latter is not

only important for possible future applications in the field of plasmonics, where graphene seems to be a promising material,³⁴ but also because of fundamental reasons. Recent experiments and theoretical studies showed that interactions between charge carriers and plasmons in graphene, forming so-called plasmarons, yield to measurable changes in the energy spectrum.³⁵

The paper is organized as follows. In Sec. II, we introduce the model Hamiltonian including the eigensystem and summarize the formalism of the random phase approximation (RPA). In Sec. III, analytical and numerical results for the free polarization function of the undoped and the doped system are given. In Sec. IV, the dielectric function is used to analyze the static screening properties due to charged impurities. We provide qualitatively the asymptotic behavior of the induced potential. The long-wavelength collective charge excitations of graphene are derived in Sec. V and afterwards compared to the numerical result. We find the existence of several new potential plasmon modes that are absent without any spin-orbit interactions. Most of these zeros, however, are overdamped as can be seen from the energy loss function. We close with conclusions and outlook in Sec. VI. Finally, in Appendices A and B we give details of the calculation of the free polarization function.

II. THE MODEL

We describe graphene with SOI within the Dirac cone approximation. At one K point, the Hamiltonian is given by³

$$\hat{H} = v_F \mathbf{p} \cdot \boldsymbol{\tau} + \lambda_R (\boldsymbol{\tau} \times \boldsymbol{\sigma}) \cdot \mathbf{e}_z + \lambda_I \tau_z \sigma_z. \quad (1)$$

The Pauli matrices $\boldsymbol{\tau}$ ($\boldsymbol{\sigma}$) act on the pseudospin (real spin) space. The other K point can be described by the above Hamiltonian with $\sigma_x \rightarrow -\sigma_x$ and $\sigma_z \rightarrow -\sigma_z$. Since the two K points are not coupled, we can limit our discussion to the above Hamiltonian, multiplying the final results by the valley index $g_v = 2$. Moreover, without loss of generality, we assume a positive Rashba and intrinsic coupling as the eigensystem and thus the dielectric function is not changed for negative values.

A. Solution

For a sufficiently large intrinsic coupling parameter, $\lambda_I > \lambda_R$, the system is in the spin quantum Hall phase with a characteristic band gap. For $\lambda_R > \lambda_I$ the gap in the spectrum is closed and the system behaves as an ordinary semimetal. At the point where $\lambda_R = \lambda_I$ a quantum phase transition occurs in the system. In the following we mainly set $v_F = 1$ and $\hbar = 1$.

The eigensystem reads

$$|\chi_{\pm\pm}(\mathbf{k})\rangle = \frac{1}{\sqrt{2}} \begin{pmatrix} \sin(\theta_{\mp}/2) \\ \cos(\theta_{\mp}/2)e^{i\varphi} \\ \pm \cos(\theta_{\mp}/2)e^{i\varphi} \\ \pm \sin(\theta_{\mp}/2)e^{2i\varphi} \end{pmatrix}, \quad (2)$$

$$|\chi_{\pm\mp}(\mathbf{k})\rangle = \frac{1}{\sqrt{2}} \begin{pmatrix} \cos(\theta_{\mp}/2) \\ -\sin(\theta_{\mp}/2)e^{i\varphi} \\ \mp \sin(\theta_{\mp}/2)e^{i\varphi} \\ \pm \cos(\theta_{\mp}/2)e^{2i\varphi} \end{pmatrix},$$

with $\sin(\theta_{\pm}) = k/\sqrt{k^2 + \lambda_{\pm}^2}$ and $\lambda_{\alpha} = \lambda_R + \alpha\lambda_I$, and ($k = |\mathbf{k}|$)

$$E_{\alpha\beta}(\mathbf{k}) = \alpha\lambda_R + \beta\sqrt{k^2 + \lambda_{-\alpha}^2} \quad (\alpha, \beta = \pm 1). \quad (3)$$

For $\lambda_R \neq 0$ the spin degeneracy is lifted and two distinct Fermi wave vectors, $k_{F\pm} = \sqrt{\mu(\mu \mp 2\lambda_R) \pm 2\lambda_R\lambda_I - \lambda_I^2}$, exist. In Fig. 1, the energy dispersion is shown for three characteristic values of the SOI.

The energy scales for the SOC parameters in monolayer graphene, $\lambda_I = 12 \mu\text{eV}$ and $\lambda_R = 5 \mu\text{eV}$ for an electric field of 1 V/nm, are generally small.³⁶ However, it was shown that these parameters can be enlarged to $\lambda_I \approx 30 \text{ meV}$ for thallium adatoms²⁹ or $\lambda_R \approx 13 \text{ meV}$ for graphene placed on a Ni(111) surface.³¹

The above Hamiltonian with only Rashba coupling can be mapped onto the bilayer Hamiltonian without SOI, relating the interlayer hopping parameter $t_{IL} \approx 0.2 \text{ eV}$ ³⁷ to the Rashba SOC. Our findings can also be applied to a topological insulator within the Kane-Mele model.³

B. Dielectric function

In order to find the dielectric function in RPA³⁸ given by

$$\varepsilon(q, \omega) = 1 - V(q)\chi_0(q, \omega), \quad (4)$$

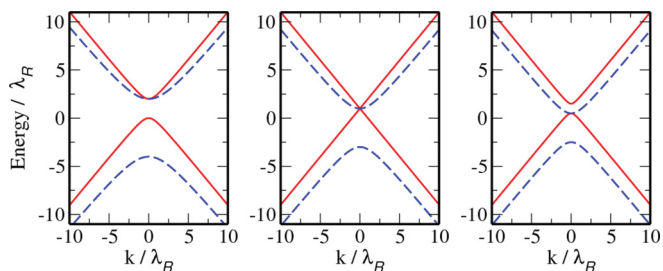


FIG. 1. (Color online) Energy dispersion in units of λ_R for $E_{+\pm}$ (solid lines) and $E_{-\pm}$ (dashed lines): (a) $\lambda_I = 2\lambda_R$, (b) $\lambda_I = \lambda_R$, (c) $\lambda_I = \lambda_R/2$.

where $V(q) = e^2/2\epsilon_0 q$ is the Fourier transform of the Coulomb potential in two dimensions, $V(r) = e^2/4\pi\epsilon_0 r$, and ϵ_0 the vacuum permittivity, one needs to calculate the free polarization,

$$\chi_0(q, \omega) = \sum_{\alpha, \eta_i = \pm 1} \int \frac{g_v d^2 k}{(2\pi)^2} |(\chi_{\eta_1 \eta_2}(\mathbf{k}) | \chi_{\eta_3 \eta_4}(\mathbf{k} + \mathbf{q}))|^2 \times \frac{\alpha f(E_{\eta_1 \eta_2}(\mathbf{k}))}{\omega - \alpha[E_{\eta_3 \eta_4}(\mathbf{k} + \mathbf{q}) - E_{\eta_1 \eta_2}(\mathbf{k})] + i0}. \quad (5)$$

In the following we assume zero temperature. The Fermi function $f(E)$ then reduces to a simple step function. Because of the general relation $\chi_0(q, -\omega) = [\chi_0(q, \omega)]^*$, we restrict our discussions to positive frequencies ω .

III. ANALYTICAL RESULTS

A. Zero doping

For zero doping the valence bands are completely filled while the conduction bands are empty. Only transitions between bands $E_{\alpha-}$ and $E_{\beta+}$ are possible. The resulting charge correlation function can be decomposed as

$$\bar{\chi}_0(q, \omega) = \sum_{\eta_i = \pm} \chi^{\eta_1 \rightarrow \eta_3+}(q, \omega). \quad (6)$$

Here we introduced the notation $\chi^{\eta_1 \eta_2 \rightarrow \eta_3 \eta_4}(q, \omega)$ describing transitions from the initial band $E_{\eta_1 \eta_2}(\mathbf{k})$ to the final band $E_{\eta_3 \eta_4}(\mathbf{k} + \mathbf{q})$. For the imaginary part we find

$$\text{Im}\{\chi^{\mp \rightarrow \mp+}(q, \omega)\} = \frac{g_v}{16} \theta[\omega^2 - q^2 - 4\lambda_{\pm}^2] \times \left[\frac{3q^4 - 4\lambda_{\pm}^2 q^2 - 5q^2 \omega^2 + 2\omega^4}{(\omega^2 - q^2)^{3/2}} - \frac{|q^2 - \omega(\omega - 2\lambda_{\pm})| + |q^2 - \omega(\omega + 2\lambda_{\pm})|}{\omega} \right] \quad (7)$$

and

$$\text{Im}\{\chi^{\pm \rightarrow \mp+}(q, \omega)\} = -\frac{g_v}{8} \theta[\omega_{\pm}^2 - q^2 - 4\gamma^2] \left[\sqrt{\omega_{\pm}^2 - q^2} - \frac{|q^2 - \omega(\omega \pm 2\lambda_{-})|}{2\omega} - \frac{|q^2 - \omega(\omega \pm 2\lambda_{+})|}{2\omega} \right]. \quad (8)$$

Here we defined $\omega_{\pm} = \omega \pm 2\lambda_R$ and $\gamma = \max\{\lambda_R, \lambda_I\}$. For equally large spin-orbit coupling parameters, $\lambda_R = \lambda_I$, the imaginary part is divergent at the threshold $\omega = q$ but finite otherwise. The divergent part of the polarization is $\chi^{+\rightarrow++}$ as the bands $E_{+\pm}(\mathbf{k})$ are linear in momentum.

The real part can be obtained via the Kramers-Kronig relations

$$\text{Re}\{\bar{\chi}_0(q, \omega)\} = \frac{2}{\pi} \mathcal{P} \int_0^{\infty} d\omega' \frac{\omega' \text{Im}\{\bar{\chi}_0(q, \omega')\}}{\omega'^2 - \omega^2}. \quad (9)$$

After carrying out the remaining integration, where it is necessary to keep the principal value, we arrive at

$$\begin{aligned} \text{Re}\{\chi^{\mp \rightarrow \mp}(q, \omega)\} = & \frac{g_v}{8\pi} \left[-2\lambda_{\pm} + 2\sqrt{q^2 + \lambda_{\pm}^2} (5q^2\omega^2 + 4q^2\lambda_{\pm}^2 - 3q^4 - 2\omega^4) \text{Re} \left\{ \frac{\arctan\left(\frac{\sqrt{q^2 - \omega^2}}{2\lambda_{\pm}}\right)}{(q^2 - \omega^2)^{3/2}} \right\} \right. \\ & \left. - \frac{2q^2\lambda_{\pm}}{q^2 - \omega^2} + 2\lambda_{\pm} \ln \left| \frac{q^2 - \omega^2 + 4\lambda_{\pm}^2}{(\sqrt{q^2 + \lambda_{\pm}^2} + \lambda_{\pm})^2 - \omega^2} \right| - \frac{\omega^2 - q^2}{2\omega} \ln \frac{\sqrt{q^2 + \lambda_{\pm}^2} + \lambda_{\pm} + \omega}{\sqrt{q^2 + \lambda_{\pm}^2} + \lambda_{\pm} - \omega} \right] \end{aligned} \quad (10)$$

and

$$\begin{aligned} \text{Re}\{\chi^{\pm \rightarrow \mp}(q, \omega)\} = & -\frac{g}{4\pi} \left[2(\pm\lambda_R - \gamma \pm \lambda_R \ln 4) \mp 2\lambda_R \text{arcsinh}\left(\frac{2\gamma}{q}\right) \right. \\ & - \frac{1}{2} \text{Re} \left\{ \sqrt{q^2 - \omega_{\pm}^2} \arcsin \frac{\sqrt{q^2 - \omega_{\pm}^2} [q + \omega_{\pm} (2\gamma - \sqrt{q^2 + 4\gamma^2})]}{\sqrt{q^2 + 4\gamma^2} - \omega_{\pm}} \right\} \\ & - \frac{1}{2} \text{Re} \left\{ \sqrt{q^2 - \omega_{\mp}^2} \arcsin \frac{\sqrt{q^2 - \omega_{\mp}^2} [q - \omega_{\mp} (2\gamma - \sqrt{q^2 + 4\gamma^2})]}{\sqrt{q^2 + 4\gamma^2} + \omega_{\mp}} \right\} \\ & + \theta[\pm\lambda_{\pm}] \mathcal{L}_{(\pm\lambda_{\mp})}(\sqrt{q^2 + \lambda_{\mp}^2} \mp \lambda_{\mp}) - \frac{1}{2} \text{sign}(\pm\lambda_{\pm}) \mathcal{L}_{(\pm\lambda_{\mp})}(\sqrt{q^2 + 4\gamma^2} \mp 2\lambda_R) \\ & \left. + \theta[\pm\lambda_{\mp}] \mathcal{L}_{(\pm\lambda_{\pm})}(\sqrt{q^2 + \lambda_{\pm}^2} \mp \lambda_{\pm}) - \frac{1}{2} \text{sign}(\pm\lambda_{\mp}) \mathcal{L}_{(\pm\lambda_{\pm})}(\sqrt{q^2 + 4\gamma^2} \mp 2\lambda_R) \right]. \end{aligned} \quad (11)$$

Here we defined the function

$$\mathcal{L}_{\lambda}(x) = x + \lambda \ln \frac{x^2 - \omega^2}{q^2} - \frac{\omega^2 - q^2}{2\omega} \ln \left| \frac{x + \omega}{x - \omega} \right|. \quad (12)$$

B. Finite doping

We now continue with the case of a finite chemical potential lying in the conduction band (the p -doped case is analogous). The free polarization in the doped case reads

$$\chi_0(q, \omega) = \bar{\chi}_0(q, \omega) + \delta\chi_{k_{F+}}(q, \omega) + \delta\chi_{k_{F-}}(q, \omega). \quad (13)$$

$\bar{\chi}_0$ is the undoped part given above. The two remaining contributions, $\delta\chi_{k_{F+}}$ and $\delta\chi_{k_{F-}}$, with

$$\begin{aligned} \delta\chi_{k_{F\pm}}(q, \omega) = & \frac{g_v}{4\pi^2} \sum_{\alpha, \mu, \nu = \pm 1} \mathcal{P} \int_0^{k_{F\pm}} d^2k \\ & \times \sum_{\alpha = \pm 1} \frac{\alpha |\langle \chi_{\pm\alpha}(\mathbf{k}) | \chi_{\mu\nu}(\mathbf{k} + \mathbf{q}) \rangle|^2}{\omega + i0 - \alpha [E_{\mu\nu}(\mathbf{k} + \mathbf{q}) - E_{\pm\alpha}(\mathbf{k})]}, \end{aligned} \quad (14)$$

refer to transitions with initial states in band E_{++} and E_{--} , respectively. As the expressions for the extrinsic real and imaginary part of the free polarization function are quite lengthy, we refer to Appendix B where the results including major steps of the derivation can be found.

Similar to the undoped case, the density correlation function of graphene is finite at $\omega = q$ for $\lambda_R \neq \lambda_I$ and divergent for $\lambda_R = \lambda_I$. However, this divergence vanishes in the RPA improved result.⁸

From the shape of the Fermi surface and the dispersion relation as given in Eq. (3), we can determine the boundaries

of the dissipative electron-hole continuum.³⁸ In Fig. 2 this is shown for the particular choice of $\lambda_R = 2\lambda_I = 0.3\mu$. In general, the lower and upper boundaries of the damped region I are given by

$$\omega_{\text{low}}^I = \max\{0, \sqrt{(k_{F-} - q)^2 + \lambda_{+}^2} - \sqrt{k_{F-}^2 + \lambda_{+}^2}\}$$

and

$$\omega_{\text{up}}^I = \max\{\sqrt{(k_{F-} + q)^2 + \lambda_{+}^2} - \sqrt{k_{F-}^2 + \lambda_{+}^2}, \sqrt{(k_{F+} + q)^2 + \lambda_{-}^2} - \sqrt{k_{F+}^2 + \lambda_{-}^2}\},$$

respectively. Region I is due to intraband transitions from band $E_{\pm+}(\mathbf{k})$ to $E_{\pm+}(\mathbf{k} + \mathbf{q})$. Region II accounts for interband

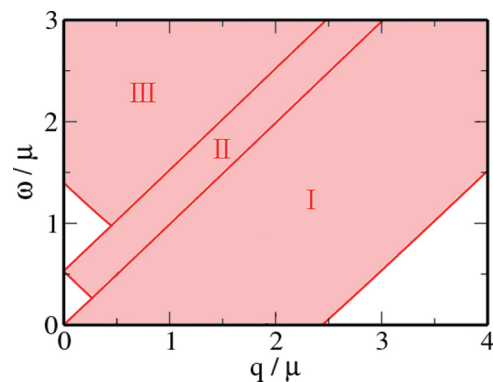


FIG. 2. (Color online) Single-particle continuum (dark area) for the particular choice of $\lambda_R = 2\lambda_I = 0.3\mu$. Analytical expressions for the boundaries of the distinct regions I, II, and III can be found in Sec. III B.

transitions between conduction bands and is confined by

$$\omega_{\text{up/low}}^{\text{II}} = \sqrt{(k_{F\pm} \pm q)^2 + \lambda_{\pm}^2} - \sqrt{k_{F-}^2 + \lambda_{+}^2} + 2\lambda_R.$$

For region III the lower limit reads

$$\omega_{\text{low}}^{\text{III}} = \min\left\{\sqrt{(k_{F-} - q)^2 + \lambda_{+}^2} + \sqrt{k_{F-}^2 + \lambda_{+}^2} - 2\lambda_R, \sqrt{(k_{F+} - q)^2 + \lambda_{-}^2} + \sqrt{k_{F+}^2 + \lambda_{-}^2}\right\},$$

while there is no restriction to the upper boundary. This part is due to transitions between valence and conduction bands.

IV. SCREENING OF IMPURITIES

The potential of a screened charged impurity is obtained from the definition of the dielectric function,

$$\Phi(r) = \frac{Q}{\epsilon_0} \int_0^{\infty} dq \frac{J_0(qr)}{\epsilon(q,0)}. \quad (15)$$

$J_0(x)$ is the Bessel function of the first kind and Q the charge of the impurity. Making use of Eq. (15) the screened potential for the undoped system is calculated numerically where $\Phi(r)$ is mainly determined by the long-wavelength behavior of the static correlator.¹⁸ As can be seen from Fig. 3(a), the long-wavelength limit of the polarization $\bar{\chi}_0(0,0)$ is finite in the semimetallic state ($\lambda_R > \lambda_I$) and zero otherwise while for large momenta all functions scale like $1/q$. From Fig. 4(a) we can see that for $\lambda_I \gtrsim \lambda_R$ the potential scales like $\Phi(r) \propto 1/r$ at large distances. For $\lambda_R > \lambda_I$ the asymptotic potential behaves as $\Phi(r) \propto 1/r^3$; see Fig. 4(b). The actual values of μr at which the above asymptotics are appropriate approximations depend on the difference of λ_R and λ_I . As mentioned in the introduction, the two different parameter regimes belong to different phases separated by the quantum critical point at $\lambda_R = \lambda_I$.

The static density correlator for the doped system is much more complicated. Integrals of the form (15) are usually

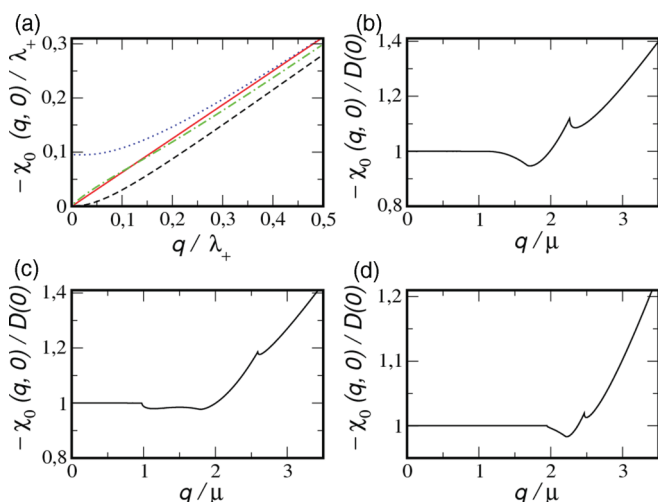


FIG. 3. (Color online) Static real part of the charge susceptibility for (a) undoped graphene with fixed λ_+ for $\lambda_R = 2\lambda_I$ (dotted), $\lambda_R = \lambda_I$ (dot-dashed), $\lambda_I = 2\lambda_R$ (dashed), $\lambda_R = \lambda_I = 0$ (straight), and doped graphene with (b) $\lambda_R = \lambda_I = 0.3\mu$, (c) $\lambda_R = 2\lambda_I = 0.3\mu$, and (d) $2\lambda_R = \lambda_I = 0.3\mu$ in units of the density of states $D(0) = g_v\mu/\pi$.

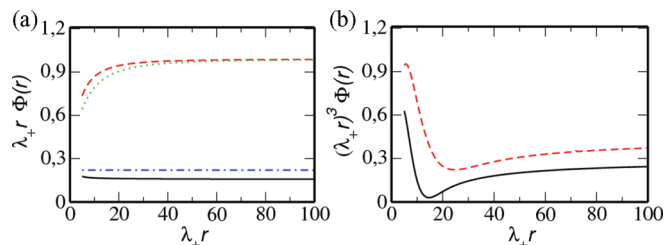


FIG. 4. (Color online) Asymptotic screened potential (in units of $Q\lambda_+/\epsilon_0$) of undoped graphene for fixed $\lambda_+ = \lambda_R + \lambda_I$ and different spin-orbit coupling parameters. (a) $\lambda_R = \lambda_I$ (straight line), $\lambda_I = 2\lambda_R$ (dashed), $\lambda_R = 0$ (dotted). Also shown is the noninteracting case $\lambda_R = \lambda_I = 0$ (dot-dashed). (b) $\lambda_I = 0$ (straight), $\lambda_R = 2\lambda_I$ (dashed).

treated analytically by approximating the Bessel function by its asymptotic values. The subsequent Fourier integral can then be solved with the Lighthill theorem.³⁹ The above theorem states that singularities in the derivatives of the dielectric function give rise to a characteristic, algebraic, oscillating decay of the screened potential. Physically, these Friedel oscillations are due to backscattering on the Fermi surface. We can thus make qualitative predictions for the potential $\Phi(r)$ at large distances away from the impurity, only from the analytical structure of the polarization function without carrying out the integration. Afterwards these predictions are compared to the exact numerical solution.

For nonzero SOC and $\lambda_R \neq \lambda_I$ the first derivative of the polarization function is singular at special points $q = 2k_{F\pm}$; see Figs. 3(c) and 3(d). According to the Lighthill theorem the potential will exhibit a superposition of two different kinds of oscillations whereat $\Phi(r) \propto 1/r^2$. This beating should be observable in sufficiently clean samples if the Rashba parameter, and the consequential breaking of the spin-degeneracy, is large enough. For predominant intrinsic SOI, the two oscillatory parts interfere constructively finally yielding an additional spin-degeneracy factor of $g_s = 2$.¹⁴ For $\lambda_R = \lambda_I$ already the first derivative of $\chi_0(q,0)$ is singular at $q = 2k_{F-}$ while at $q = 2k_{F+}$ only the second derivative diverges; see Fig. 3(b). The main contribution in the potential again will be of order $1/r^2$. The numerical inspection of $\Phi(r)$ as displayed in Fig. 5 confirms the above predictions.

The resulting potential deviates significantly from the

$$\Phi(r) \propto \frac{\cos(2k_F r)}{(2k_F r)^3} \quad (16)$$

behavior of standard graphene within the Dirac cone approximation.^{8,40}

Nevertheless, including the full dispersion of graphene can also lead to a different decay behavior, i.e., to anisotropic regular Friedel oscillations decaying like $1/r^2$.⁴¹

V. PLASMONS

Plasmons are defined as the zeros of the dielectric function,

$$\epsilon(q, \omega_p - i\gamma) = 0. \quad (17)$$

For small damping constant γ , Eq. (17) can be substituted by the approximate equation³⁸

$$\text{Re}\{\epsilon(q, \omega_p)\} = 0. \quad (18)$$

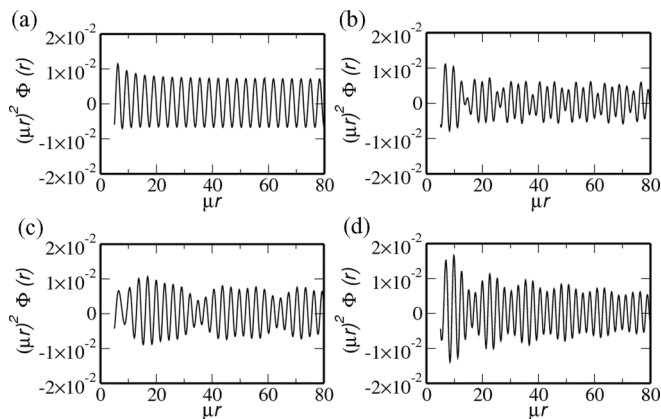


FIG. 5. Asymptotic screened potential (in units of $Q\mu/\epsilon_0$) of doped graphene for various spin-orbit coupling parameters: (a) $(\lambda_R/\mu, \lambda_I/\mu) = (0, 0.3)$, (b) $(0.3, 0.15)$, (c) $(0.15, 0.3)$, and (d) $(0.3, 0.3)$.

Only if γ is small compared to ω_p , one can speak of collective density fluctuations. For large Landau damping, it is thus important to also discuss the more general energy loss function $\text{Im}\{-1/\epsilon(q, \omega)\}$ which gives the spectral density of the internal excitations of the system.

Similar to Refs. 14 and 18, there are several solutions of Eq. (18) for nonzero SOC parameters. In Fig. 6, these solutions are shown as straight lines together with a density plot of the energy loss function $\text{Im}\{-1/\epsilon(q, \omega)\}$. One of these solutions has an almost linear dispersion with a sound velocity close to the Fermi velocity which exhibits an ending point for $\lambda_R \sim \lambda_I$ associated with a double zero of the real part of the dielectric function. However, as can be seen from Figs. 7(a) and 7(b), this solution does not yield to a resonance in the loss function and does thus not resemble a plasmonic mode. In the case where the gap in the spectrum is closed ($\lambda_R > \lambda_I$), two additional zeros appear leading to potential

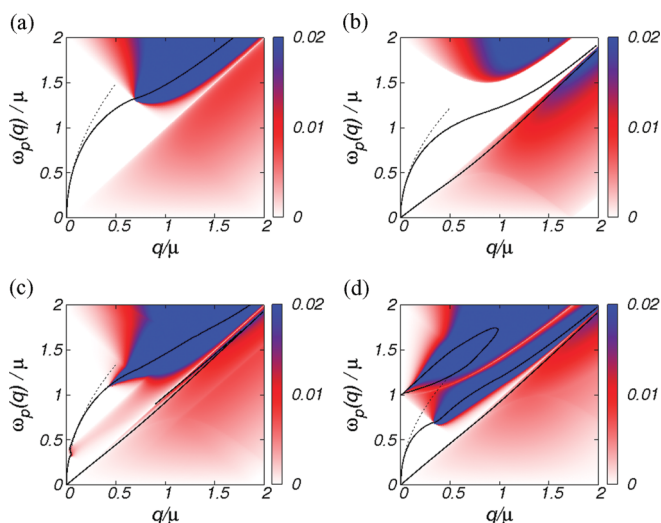


FIG. 6. (Color online) Density plot of $\text{Im}\{-1/\epsilon(q, \omega)\}$ for various spin-orbit coupling parameters: (a) $(\lambda_R/\mu, \lambda_I/\mu) = (0, 0)$, (b) $(0, 0.5)$, (c) $(0.25, 0.25)$, (d) $(0.5, 0)$. Straight lines correspond to the numerically calculated zeros of the real part of the dielectric function while dashed lines represent the long-wavelength result of Eq. (19).

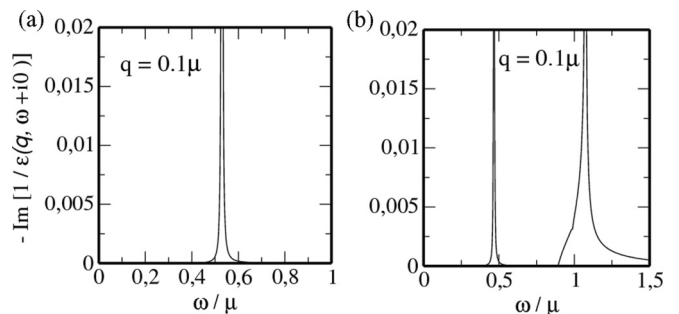


FIG. 7. Energy loss function $\text{Im}\{-1/\epsilon(q, \omega + i0)\}$ for fixed $q = 0.1\mu$ with (a) $\lambda_R = 0, \lambda_I = 0.5\mu$ and (b) $\lambda_R = 0.5\mu, \lambda_I = 0$.

high-energy modes similar to bilayer graphene.^{18,19} However, these potential collective modes are damped by interband transitions; i.e., the corresponding peaks in the loss function are broadened out as can be seen from Fig. 7(b) and no clear signature is seen in the density plot.

We are thus left with the branch which is also present for “clean” graphene and which resembles the only genuine plasmonic mode; see Fig. 6(a). Its dispersion ω_p can be approximated in the long-wavelength limit ($q \ll \omega$) by⁴²

$$\omega_p^0(q) = \beta\sqrt{q}, \quad (19)$$

where the prefactor is given by $\beta = \sqrt{\frac{g_v e^2}{8\pi\epsilon_0} \sum_{\mu=\pm 1} \frac{k_{F\mu}^2}{\sqrt{k_{F\mu}^2 + \lambda_{\pm\mu}^2}}}$. We thus recover the typical \sqrt{q} dispersion of 2D plasmons.

The long-wavelength approximation is shown as a dashed line in Fig. 6 and coincides with the numerical solution, ω_p , for small momenta, whereas for larger momenta, the ω_p is redshifted compared to ω_p^0 . If λ_I is large enough, ω_p remains in the region where Landau damping is absent, see Fig. 6(b),¹⁴ otherwise it eventually enters the Landau-damped region due to interband transitions from the valence to the conduction band, see Figs. 6(a) and 6(d).

For two occupied conduction bands, which is the case in Fig. 6(c) and in Fig. 8, the plasmon mode is disrupted at $q \approx 0.05\mu$ by a region with a finite imaginary part where it becomes damped. This additional Landau-damped region is due to interband transitions from the two conduction bands. The analytical description of the boundaries of this region can be found in Sec. III B.

This “pseudogap” of the plasmon dispersion can also be obtained from only considering Eq. (18) since the “plasmon” velocity formally diverges at the entering and exit point as can be seen from Fig. 6(c). The crossing points can alternatively be approximated by looking at the intersection of this region with the analytical long-wavelength approximation of the analytic plasmon dispersion. For the quantum critical point ($\lambda_R = \lambda_I$), this leads to the critical wave vector

$$q_{\text{cr}}^{\pm} = \frac{(\beta - \sqrt{\beta^2 \mp 4(k_{F-} - \sqrt{k_{F-}^2 + 4\lambda_R^2 + 2\lambda_R})})^2}{4},$$

and in particular to $q_{\text{cr}}^- \approx 0.019\mu$ and $q_{\text{cr}}^+ \approx 0.025\mu$ for $\lambda_{R/I} = 0.25\mu$. For a proper analysis, the full energy loss function thus needs to be discussed which is done in Fig. 9. It shows how the spectral weight is eventually transferred from the lower to

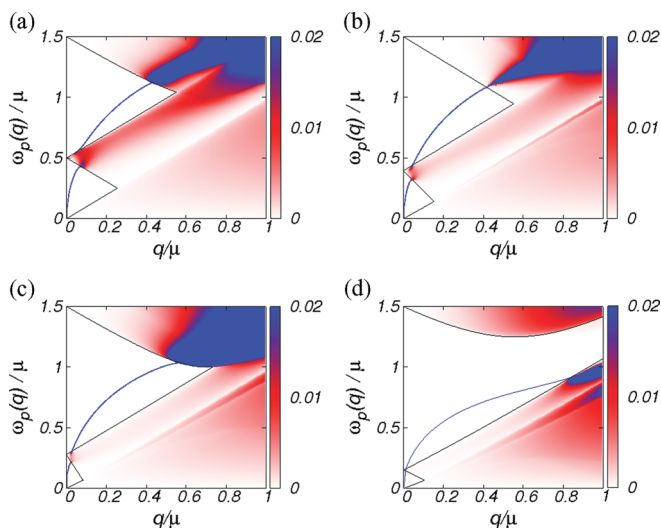


FIG. 8. (Color online) Energy loss function $\text{Im}\{-1/\varepsilon(q, \omega + i0)\}$ for (a) $(\lambda_R/\mu, \lambda_I/\mu) = (0.25, 0)$, (b) $(0.25, 0.25)$, (c) $(0.25, 0.5)$, and (d) $(0.25, 0.75)$. The straight blue lines show the undamped plasmon modes. The black lines indicate the boundaries of the single-particle continuum (see Sec. III B).

the upper band as momentum is increased, explaining the step in the plasmon spectrum as shown in Fig. 8.

The pseudogap of the plasmonic mode always appears for $\lambda_R < 0.5\mu$, since then two conduction bands are occupied independently of the value of λ_I , but it decreases for increasing λ_I as the dissipative region due to interband transitions diminishes. In the opposite case of $\lambda_R > 0.5\mu$, either one or two bands can be occupied. For zero intrinsic coupling, the pseudogap is absent but increases up to a maximum value at around $\lambda_I \approx \lambda_R$ for increasing λ_I .

Let us close with a comment on plasmons in undoped graphene. For neutral monolayer graphene and at zero temperature, plasmons can exist if one takes into account a circularly polarized light field²⁴ or effects beyond RPA,⁴³ and in bilayer by including trigonal warping.⁴⁴ In our system, the real part of the dielectric function is always nonzero for the undoped case and thus no plasmons exist.

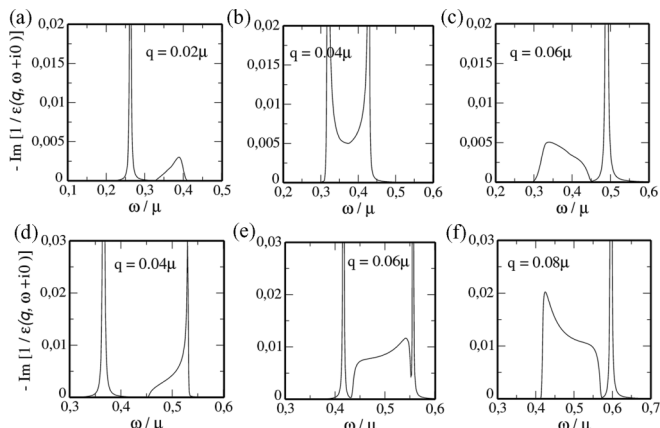


FIG. 9. Top: Energy loss function $\text{Im}\{-1/\varepsilon(q, \omega + i0)\}$ for $\lambda_R = \lambda_I = 0.25\mu$ and various wave vectors q . Bottom: The same for $\lambda_R = 0.25\mu$ and $\lambda_I = 0$.

VI. CONCLUSIONS AND OUTLOOK

We have presented analytical and numerical results for the dielectric function of monolayer graphene in the presence of Rashba and intrinsic spin-orbit interactions within the random phase approximation for finite frequency, wave vector, and doping. The cases of predominant Rashba and intrinsic coupling and the case of equally large SOC were opposed.

In the static limit the screening properties due to external impurities were studied. Our findings show that the power-law dependence of the screened potential in the undoped system depends on the ratio of the Rashba and intrinsic parameters. While for $\lambda_R > \lambda_I$ the screened potential scales like $\Phi(r) \propto 1/r^3$, for $\lambda_I \geq \lambda_R$ a weaker screening, $\Phi(r) \propto 1/r$, was found. For finite Rashba coupling, a beating of Friedel oscillations in the doped system occurs due to the existence of two distinct kinds of Fermi wave vectors. For large $\lambda_I \gg \lambda_R$, this beating vanishes and the two contributions interfere constructively.

In the last section the influence of SOI on the collective charge excitations was discussed. We found that while only one plasmon mode exists for standard graphene, several new potential modes occur for finite SOC. However, most of these modes are overdamped and can hardly be detected as they lie in the region with finite Landau damping. In the case when the two conduction bands are filled, the undamped plasmon mode is disrupted by a narrow dissipative region strip due to particle-hole excitations. This “pseudogap” might be useful to gain further control in possible plasmonic circuitries based on graphene.

As already mentioned in the beginning, our findings go even beyond monolayer graphene. For purely Rashba coupling the dielectric function presented in this work equals that of bilayer graphene. The role of the SOC parameter is then played by the interlayer hopping amplitude t_{IL} being several orders of magnitude larger than λ_R . Additionally, the Hamiltonian in Eq. (1) generally describes a system known as the Kane-Mele topological insulator.³ Our discussion can thus be fully adopted to materials modeled by this Hamiltonian. Besides that, our findings might also be relevant for other monolayers with similar symmetry properties compared to those of graphene, e.g. MoS₂, where SOC is naturally strong.⁴⁶ A detailed study of the dielectric properties of MoS₂, however, is left open for future works.

ACKNOWLEDGMENTS

We thank G. Gómez-Santos and O. V. Gamayun for useful discussions and comments. This work was supported by Deutsche Forschungsgemeinschaft via Grant No. GRK 1570, by FCT under Grant No. PTDC/FIS/101434/2008, and MIC under Grant No. FIS2010-21883-C02-02.

APPENDIX A: DETAILS OF THE CALCULATION OF THE UNDOPE POLARIZATION

The undoped polarization is composed of four parts,

$$\bar{\chi}_0(q, \omega) = \sum_{\eta_i = \pm} \chi^{\eta_1 \rightarrow \eta_3 +}(q, \omega). \quad (\text{A1})$$

As two of them can be obtained by a simple substitution, i.e., $\chi_{\lambda_R}^{+ \rightarrow + +}(q, \omega) = \chi_{-\lambda_R}^{+ \rightarrow - +}(q, \omega)$ and $\chi_{\lambda_R}^{+ \rightarrow - +}(q, \omega) = \chi_{-\lambda_R}^{- \rightarrow - +}(q, \omega)$, only two contributions remain. With the help

of the Dirac identity the imaginary parts read

$$\text{Im}\{\chi^{-\rightarrow-\rightarrow+}(q,\omega)\} = -\frac{g_v}{4\pi} \int d^2k \sum_{\alpha=\pm 1} \alpha |\langle \chi_{-\alpha}(\mathbf{k}) | \chi_{-\alpha}(\mathbf{k} + \mathbf{q}) \rangle|^2 \delta[\omega - \alpha(E_{-\alpha}(\mathbf{k} + \mathbf{q}) - E_{-\alpha}(\mathbf{k}))] \quad (\text{A2})$$

$$= \frac{g_v}{16} \theta[\omega^2 - q^2 - 4\lambda_+^2] \left[\frac{3q^4 - 4\lambda_+^2 q^2 - 5q^2 \omega^2 + 2\omega^4}{(\omega^2 - q^2)^{3/2}} - \frac{|q^2 - \omega(\omega - 2\lambda_+)| + |q^2 - \omega(\omega + 2\lambda_+)|}{\omega} \right] \quad (\text{A3})$$

and

$$\text{Im}\{\chi^{+\rightarrow-\rightarrow+}(q,\omega)\} = -\frac{g_v}{4\pi} \int d^2k \sum_{\alpha=\pm 1} \alpha |\langle \chi_{+\alpha}(\mathbf{k}) | \chi_{-\alpha}(\mathbf{k} + \mathbf{q}) \rangle|^2 \delta[\omega - \alpha(E_{-\alpha}(\mathbf{k} + \mathbf{q}) - E_{+\alpha}(\mathbf{k}))] \quad (\text{A4})$$

$$= -\frac{g_v}{8\pi} \int_{|\lambda_-|}^{\infty} dy \frac{\sqrt{\omega_+^2 - q^2} \sqrt{\frac{q^2(q^2 - \omega_+^2 + 4\lambda_+^2)(q^2 - \omega_+^2 + 4\lambda_-^2)}{(q^2 - \omega_+^2)^2}} - \left[y - \frac{\omega_+}{2} \left(1 + \frac{4\lambda_R \lambda_I}{q^2 - \omega_+^2} \right) \right]^2}{(y - \lambda_-)(\omega - y + \lambda_-)} \times \theta \left[1 - \left(\frac{\omega_+^2 - q^2 - 2\omega_+ y - 4\lambda_R \lambda_I}{2q\sqrt{y^2 - \lambda_-^2}} \right)^2 \right] \theta[\omega_+^2 - q^2 - 4\gamma^2] \quad (\text{A5})$$

$$= -\frac{g_v}{8} \theta[\omega_{\pm}^2 - q^2 - 4\gamma^2] \left[\sqrt{\omega_{\pm}^2 - q^2} - \frac{|q^2 - \omega(\omega \pm 2\lambda_-)|}{2\omega} - \frac{|q^2 - \omega(\omega \pm 2\lambda_+)|}{2\omega} \right] \quad (\text{A6})$$

with $\gamma = \max\{\lambda_R, \lambda_I\}$ and $y = \sqrt{k^2 + \lambda_-^2}$.

We can now make use of Eq. (9) in order to find the real part. The first contribution reads

$$\text{Re}\{\chi^{-\rightarrow-\rightarrow+}(q,\omega)\} = \frac{2}{\pi} \mathcal{P} \int_0^{\infty} d\omega' \frac{\omega'}{\omega^2 - \omega'^2} \text{Im}\{\chi^{-\rightarrow-\rightarrow+}(q,\omega')\} \quad (\text{A7})$$

$$= \frac{g_v}{8\pi} \left\{ -K_{\lambda}(4\lambda^2) + \mathcal{L}_{\lambda}(\sqrt{q^2 + 4\lambda^2}) + 2\mathcal{L}_{-\lambda}(\sqrt{q^2 + \lambda^2} + \lambda) - \mathcal{L}_{-\lambda}(\sqrt{q^2 + 4\lambda^2}) + \theta[q - \omega] \frac{3q^2 \omega^2 + 4q^2 \lambda^2 - 3q^4 - 2\omega^4}{(q^2 - \omega^2)^{3/2}} \frac{\pi}{2} \right\}. \quad (\text{A8})$$

Here we introduced the functions

$$K_{\lambda}(x) = 2\sqrt{x} + \frac{4q^2 \lambda^2}{(q^2 - \omega^2)\sqrt{x}} - (3q^4 - 5q^2 \omega^2 + 2\omega^4 - 4q^2 \lambda^2) \text{Re} \left\{ \frac{\arctan\left(\frac{\sqrt{x}}{\sqrt{q^2 - \omega^2}}\right)}{(q^2 - \omega^2)^{3/2}} \right\} \quad (\text{A9})$$

and

$$\mathcal{L}_{\lambda}(x) = x + \lambda \ln|x^2 - \omega^2| - \frac{\omega^2 - q^2}{2\omega} \ln \left| \frac{x + \omega}{x - \omega} \right|. \quad (\text{A10})$$

The second contribution can be solved in a similar way,

$$\begin{aligned} \text{Re}\{\chi^{+\rightarrow-\rightarrow+}(q,\omega)\} &= \frac{2}{\pi} \mathcal{P} \int_0^{\infty} d\omega' \frac{\omega'}{\omega^2 - \omega'^2} \text{Im}\{\chi^{+\rightarrow-\rightarrow+}(q,\omega')\} \\ &= -\frac{g_v}{4\pi} \left[2\lambda_R(1 + \ln 4) - \frac{1}{2} \text{Re} \left\{ \sqrt{q^2 - (\omega + 2\lambda_R)^2} \arcsin \frac{\omega + 2\lambda_R}{q} - \sqrt{q^2 - (-\omega + 2\lambda_R)^2} \right. \right. \\ &\quad \times \left. \arcsin \frac{-\omega + 2\lambda_R}{q} \right\} - \frac{1}{2} [G_{\omega/2+\lambda_R}(\sqrt{q^2 + 4\gamma^2} - \omega - 2\lambda_R) + G_{-\omega/2+\lambda_R}(\sqrt{q^2 + 4\gamma^2} + \omega - 2\lambda_R)] \\ &\quad + \theta[\lambda_R + \lambda_I] \mathcal{L}_{\lambda_-}(\sqrt{q^2 + \lambda_-^2} - \lambda_-) - \frac{1}{2} \text{sign}(\lambda_R + \lambda_I) \mathcal{L}_{\lambda_-}(\sqrt{q^2 + 4\gamma^2} - 2\lambda_R) \\ &\quad \left. + \theta[\lambda_R - \lambda_I] \mathcal{L}_{\lambda_+}(\sqrt{q^2 + \lambda_+^2} - \lambda_+) - \frac{1}{2} \text{sign}(\lambda_R - \lambda_I) \mathcal{L}_{\lambda_+}(\sqrt{q^2 + 4\gamma^2} - 2\lambda_R) \right] \quad (\text{A11}) \end{aligned}$$

with

$$G_\omega(x) = \sqrt{(x+\omega)^2 - q^2} + \omega \ln(\sqrt{(x+\omega)^2 - q^2} + x + \omega) - \sqrt{\omega^2 - q^2} \ln \frac{\omega x + \omega^2 - q^2 + \sqrt{\omega^2 - q^2} \sqrt{(x+\omega)^2 - q^2}}{x}. \quad (\text{A12})$$

APPENDIX B: DETAILS OF THE CALCULATION OF THE DOPED POLARIZATION

The extrinsic part for the band E_{-+} ,

$$\delta\chi_{k_{F-}}(q, \omega) = \frac{g_v}{4\pi^2} \sum_{\mu, \nu = \pm 1} \mathcal{P} \int_0^{k_{F-}} d^2k \sum_{\alpha = \pm 1} \frac{\alpha |\langle \chi_{-\alpha}(\mathbf{k}) | \chi_{\mu\nu}(\mathbf{k} + \mathbf{q}) \rangle|^2}{\omega + i0 - \alpha [E_{\mu\nu}(\mathbf{k} + \mathbf{q}) - E_{-\alpha}(\mathbf{k})]}, \quad (\text{B1})$$

can be summarized as

$$\begin{aligned} \delta\chi_{k_{F-}}(q, \omega) = & \frac{g_v}{4\pi^2} \mathcal{P} \int_0^{k_{F-}} d^2k \left[\frac{(\omega + i0 + \sqrt{k^2 + \lambda_+^2} + \sqrt{|\mathbf{k} + \mathbf{q}|^2 + \lambda_+^2}) |\langle \chi_{-+}(\mathbf{k}) | \chi_{--}(\mathbf{k} + \mathbf{q}) \rangle|^2}{(\omega + i0 + \sqrt{k^2 + \lambda_+^2})^2 - (|\mathbf{k} + \mathbf{q}|^2 + \lambda_+^2)} \right. \\ & + \frac{(\omega + i0 + \sqrt{k^2 + \lambda_+^2} - \sqrt{|\mathbf{k} + \mathbf{q}|^2 + \lambda_+^2}) |\langle \chi_{-+}(\mathbf{k}) | \chi_{--}(\mathbf{k} + \mathbf{q}) \rangle|^2}{(\omega + i0 + \sqrt{k^2 + \lambda_+^2})^2 - (|\mathbf{k} + \mathbf{q}|^2 + \lambda_+^2)} \\ & + \frac{(\omega_- + i0 + \sqrt{k^2 + \lambda_+^2} - \sqrt{|\mathbf{k} + \mathbf{q}|^2 + \lambda_-^2}) |\langle \chi_{-+}(\mathbf{k}) | \chi_{+-}(\mathbf{k} + \mathbf{q}) \rangle|^2}{(\omega_- + i0 + \sqrt{k^2 + \lambda_+^2})^2 - (|\mathbf{k} + \mathbf{q}|^2 + \lambda_-^2)} \\ & \left. + \frac{(\omega_- + i0 + \sqrt{k^2 + \lambda_+^2} + \sqrt{|\mathbf{k} + \mathbf{q}|^2 + \lambda_-^2}) |\langle \chi_{-+}(\mathbf{k}) | \chi_{++}(\mathbf{k} + \mathbf{q}) \rangle|^2}{(\omega_- + i0 + \sqrt{k^2 + \lambda_+^2})^2 - (|\mathbf{k} + \mathbf{q}|^2 + \lambda_-^2)} + (\omega \rightarrow -\omega) \right], \quad (\text{B2}) \end{aligned}$$

where $(\omega \rightarrow -\omega)$, and thus $(\omega_- \rightarrow -\omega_+)$, denotes terms with the sign of the frequency changed compared to the preceding expression. The corresponding expression for E_{++} can be obtained by substituting $\lambda_R \rightarrow -\lambda_R$ and $k_{F-} \rightarrow k_{F+}$. After carrying out the angle integration for the real part and choosing a proper substitution, $x = \sqrt{k^2 + \lambda_+^2} - \lambda_+$, we arrive at

$$\begin{aligned} & \text{Re} \{ \delta\chi_{k_{F-}}(q, \omega) \} \\ & = -\frac{g_v}{2\pi} \text{Re} \left\{ \mathcal{P} \int_\epsilon^{\mu - \lambda_I} dx \left[\frac{x + \lambda_R}{2x} + \frac{[q^2 - (x + \frac{\omega}{2})(x + \frac{\omega}{2} + \lambda_+)]^2}{x(x + \frac{\omega}{2})} \frac{\text{sign}(q^2 - \omega^2 - 2\omega(x + \lambda_+))}{\sqrt{q^2 - \omega^2} \sqrt{\frac{q^2}{4} (1 + \frac{4\lambda_+^2}{q^2 - \omega^2}) - (x + \frac{\omega}{2} + \lambda_+)^2}} \right. \right. \\ & \quad \left. \left. - \frac{\sqrt{q^2 - \omega^2} \sqrt{\frac{q^2}{4} \frac{(q^2 - \omega_+^2 + 4\lambda_+^2)(q^2 - \omega_+^2 + 4\lambda_R^2)}{(q^2 - \omega_+^2)^2} - [x + \frac{\omega_+}{2} (1 + \frac{4\lambda_R \lambda_I}{q^2 - \omega_+^2}) + \lambda_+]^2}}{4x(x + \omega)} \right] \right. \\ & \quad \left. \times \text{sign}(q^2 - \omega_-^2 - 2\omega_-(x + \lambda_+) - 4\lambda_R \lambda_I) \right\} + (\omega \rightarrow -\omega). \quad (\text{B3}) \end{aligned}$$

These integrals can now be solved in terms of trigonometric and hyperbolic functions.⁴⁵ In order to simplify the expressions we use the shorthand notation¹⁸

$$\hat{f}(x)|_a^b = \text{sign}(b - x)[f(b) - f(x)] - \text{sign}(a - x)[f(a) - f(x)]. \quad (\text{B4})$$

The result can then be written as

$$\begin{aligned} \text{Re} \{ \delta\chi_{k_{F-}}(q, \omega) \} = & -\frac{g_v(\mu - \lambda_I)}{2\pi} - \frac{g_v \lambda_R}{4\pi} \ln \frac{\mu - \lambda_I}{\epsilon} + \frac{g_v}{2\pi\omega} \text{Re} \left\{ \text{sign}(\omega) \left[\hat{\mathcal{R}}_1^\omega \left(\frac{q^2 - \omega^2 - 2\omega\lambda_+}{2\omega} \right) \right]_\epsilon^{\mu - \lambda_I} \right. \\ & - \hat{\mathcal{R}}_1^{-\omega} \left(\frac{q^2 + \omega^2 - 2\omega\lambda_+}{2\omega} \right) \Big|_\omega^{\mu - \lambda_I + \omega} \Big] - \text{sign}(\omega_-) \left[\hat{\mathcal{R}}_2^\omega \left(\frac{q^2 - \omega^2 + 2\lambda_- \omega}{2\omega_-} \right) \right]_\epsilon^{\mu - \lambda_I} \\ & \left. - \hat{\mathcal{R}}_2^{-\omega} \left(\frac{q^2 + \omega^2 - 2\lambda_+ \omega}{2\omega_-} \right) \Big|_\omega^{\mu - \lambda_I + \omega} \right\} + (\omega \rightarrow -\omega) \quad (\text{B5}) \end{aligned}$$

with

$$\mathcal{R}_i^\omega(x) = \frac{c_i^\omega}{\gamma_i^\omega} \sqrt{r_i^\omega} - \frac{\sqrt{\alpha_i^\omega}}{4} \ln \frac{2\alpha_i^\omega + \beta_i^\omega x + 2\sqrt{\alpha_i^\omega} \sqrt{r_i^\omega}}{x} + \frac{\tilde{c}_i^\omega}{\sqrt{\gamma_i^\omega}} \ln (2\sqrt{\gamma_i^\omega} \sqrt{r_i^\omega} + 2\gamma_i^\omega x + \beta_i^\omega) \quad (\text{B6})$$

and $r_i^\omega = \alpha_i^\omega + \beta_i^\omega x + \gamma_i^\omega x^2$. The coefficients read

$$\begin{aligned} \alpha_1^\omega &= \frac{[q^2 - \omega(\omega + 2\lambda_+)]^2}{4}, & \alpha_2^\omega &= \frac{[q^2 - \omega(\omega_- - 2 \operatorname{sign}(\omega)\lambda_I)]^2}{4}, \\ \beta_1^\omega &= (\omega^2 - q^2)(2\lambda_+ + \omega), & \beta_2^\omega &= 8\lambda_R^2 \lambda_I - 2\lambda_R \lambda_I (\omega + |\omega|) - \operatorname{sign}(\omega)(\omega - 2\lambda_R)(q^2 - \omega^2), \\ \gamma_1^\omega &= \omega^2 - q^2, & \gamma_2^\omega &= |\omega|_-^2 - q^2, & c_1^\omega &= \frac{x^2}{3} + \frac{2\lambda_+ + 7\omega}{12} x + \frac{4\lambda_+^2 - 4q^2 + 8\lambda_+^2 + 5\omega^2}{8} - \frac{2\alpha_1^\omega}{3\gamma_1^\omega}, \\ \tilde{c}_1^\omega &= \frac{\alpha_1^\omega(2\lambda_+ - \omega)}{4\gamma_1^\omega} + \frac{3\omega^3 + 6\lambda_+^2 \omega^2 - 4(q^2 + \lambda_+^2)\omega - 8\lambda_+^3}{16}, & c_2^\omega &= \frac{\gamma_2^\omega}{4}, & \tilde{c}_2^\omega &= \frac{\beta_2^\omega}{8}. \end{aligned}$$

The calculation of the imaginary part is quite similar. Starting from Eq. (B2) and carrying out the angle integration in a way similar to the real part, we arrive at

$$\begin{aligned} & \operatorname{Im} \{ \delta \chi_{k_F-}(q, \omega) \} \\ &= \frac{g_v}{2\pi} \operatorname{Re} \left\{ \mathcal{P} \int_\epsilon^{\mu-\lambda_I} dx \left[\frac{[q^2 - (x + \frac{\omega}{2})(x + \frac{\omega}{2} + \lambda_+)]^2}{x(x + \frac{\omega}{2})} \frac{\operatorname{sign}(x - \lambda_- + \omega)}{\sqrt{\omega^2 - q^2} \sqrt{\frac{q^2}{4} (1 + \frac{4\lambda_+^2}{q^2 - \omega^2}) - (x + \frac{\omega}{2} + \lambda_+)^2}} \right. \right. \\ & \quad \left. \left. - \frac{\sqrt{\omega_-^2 - q^2} \sqrt{\frac{q^2}{4} \frac{(q^2 - \omega_-^2 + 4\lambda_I^2)(q^2 - \omega_-^2 + 4\lambda_R^2)}{(q^2 - \omega_-^2)^2}} - [x + \frac{\omega_-}{2} (1 + \frac{4\lambda_R \lambda_I}{q^2 - \omega_-^2}) + \lambda_+]}{4x(x + \omega)} \operatorname{sign}(x + \lambda_+ + \omega) \right] - (\omega \rightarrow -\omega) \right\}. \quad (\text{B7}) \end{aligned}$$

The result can again be written as

$$\begin{aligned} \operatorname{Im} \{ \delta \chi_{k_F-}(q, \omega) \} &= \frac{g_v}{2\pi\omega} \operatorname{Re} \left\{ \frac{1}{i} \hat{\mathcal{R}}_1^\omega(-\lambda_+ - \omega) \Big|_\epsilon^{\mu-\lambda_I} - \frac{1}{i} \hat{\mathcal{R}}_1^\omega(-\lambda_+) \Big|_\omega^{\mu-\lambda_I+\omega} \right. \\ & \quad - \frac{1}{i} \theta[-\omega] \theta[\mu - \lambda_I + \omega] \operatorname{sign}(\lambda_+) [R_1^\omega(-\epsilon) - R_1^\omega(\epsilon)] + i \hat{\mathcal{R}}_2^\omega(\lambda_- - \omega) \Big|_\epsilon^{\mu-\lambda_I} - i \hat{\mathcal{R}}_2^\omega(\lambda_-) \Big|_\omega^{\mu-\lambda_I+\omega} \\ & \quad \left. - i \theta[-\omega] \theta[\mu - \lambda_I + \omega] \operatorname{sign}(-\lambda_-) [R_2^\omega(-\epsilon) - R_2^\omega(\epsilon)] \right\} - (\omega \rightarrow -\omega). \quad (\text{B8}) \end{aligned}$$

The limit $\epsilon \rightarrow 0$ in Eqs. (B5) and (B8) can now be taken safely giving finite results.

*To whom correspondence should be addressed: andreas.scholz@physik.uni-regensburg.de

¹P. R. Wallace, *Phys. Rev.* **71**, 622 (1947).

²A. H. Castro Neto, F. Guinea, N. M. R. Peres, K. S. Novoselov, and A. K. Geim, *Rev. Mod. Phys.* **81**, 109 (2009).

³C. L. Kane and E. J. Mele, *Phys. Rev. Lett.* **95**, 226801 (2005).

⁴M. Pletyukhov and V. Gritsev, *Phys. Rev. B* **74**, 045307 (2006).

⁵S. M. Badalyan, A. Matos-Abiague, G. Vignale, and J. Fabian, *Phys. Rev. B* **79**, 205305 (2009); **81**, 205314 (2010).

⁶C. A. Ullrich and M. E. Flatte, *Phys. Rev. B* **68**, 235310 (2003).

⁷J. Schliemann, *Phys. Rev. B* **74**, 045214 (2006); **84**, 155201 (2011); *Europhys. Lett.* **91**, 67004 (2010).

⁸B. Wunsch, T. Stauber, F. Sols, and F. Guinea, *New J. Phys.* **8**, 316 (2006).

⁹E. H. Hwang and S. Das Sarma, *Phys. Rev. B* **75**, 205418 (2007).

¹⁰A. Principi, M. Polini, and G. Vignale, *Phys. Rev. B* **80**, 075418 (2009).

¹¹T. Stauber, J. Schliemann, and N. M. R. Peres, *Phys. Rev. B* **81**, 085409 (2010).

¹²T. Stauber and G. Gomez-Santos, *Phys. Rev. B* **82**, 155412 (2010).

¹³T. Stauber, *Phys. Rev. B* **82**, 201404(R) (2010).

¹⁴P. K. Pyatkovskiy, *J. Phys.: Condens. Matter* **21**, 025506 (2009).

¹⁵X.-F. Wang and T. Chakraborty, *Phys. Rev. B* **75**, 033408 (2007).

¹⁶A. Scholz and J. Schliemann, *Phys. Rev. B* **83**, 235409 (2011).

¹⁷G. Borghi, M. Polini, R. Asgari, and A. H. MacDonald, *Phys. Rev. B* **80**, 241402(R) (2009).

¹⁸O. V. Gamayun, *Phys. Rev. B* **84**, 085112 (2011).

¹⁹S. Yuan, R. Roldan, and M. I. Katsnelson, *Phys. Rev. B* **84**, 035439 (2011).

²⁰T. Stauber and G. Gómez-Santos, *Phys. Rev. B* **85**, 075410 (2012).

²¹R. E. V. Profumo, R. Asgari, Marco Polini, and A. H. MacDonald, *Phys. Rev. B* **85**, 085443 (2012).

²²C. Triola and E. Rossi, *Phys. Rev. B* **86**, 161408 (2012).

- ²³M. H. Schultz, A. P. Jauho, and T. G. Pedersen, *Phys. Rev. B* **84**, 045428 (2011).
- ²⁴M. Busl, G. Platero, and A. P. Jauho, *Phys. Rev. B* **85**, 155449 (2012).
- ²⁵K.-H. Ding, G. Zhou, Z.-G. Zhu, and J. Berakdar, *J. Phys.: Condens. Matter* **20**, 345228 (2008).
- ²⁶P. Ingenhoven, J. Z. Bernad, U. Zülicke, and R. Egger, *Phys. Rev. B* **81**, 035421 (2010).
- ²⁷A. Hill, A. Sinner, and K. Ziegler, arXiv:1005.3211v2.
- ²⁸A. H. Castro Neto and F. Guinea, *Phys. Rev. Lett.* **103**, 026804 (2009).
- ²⁹C. Weeks, J. Hu, J. Alicea, M. Franz, and R. Wu, *Phys. Rev. X* **1**, 021001 (2011).
- ³⁰D. Ma, Z. Li, and Z. Yang, *Carbon* **50**, 297 (2012).
- ³¹A. Varykhalov, J. Sánchez-Barriga, A. M. Shikin, C. Biswas, E. Vescovo, A. Rybkin, D. Marchenko, and O. Rader, *Phys. Rev. Lett.* **101**, 157601 (2008).
- ³²Y. S. Dedkov, M. Foinin, U. Rüdiger, and C. Laubschat, *Phys. Rev. Lett.* **100**, 107602 (2008).
- ³³K.-H. Jin and S.-H. Jhi, arXiv:1206.3608v1.
- ³⁴F. Rana, *IEEE Trans. Nanotech.* **7**, 91 (2008).
- ³⁵A. Bostwick, F. Speck, T. Seyller, K. Horn, M. Polini, R. Asgari, A. H. MacDonald, and E. Rotenberg, *Science* **328**, 999 (2010).
- ³⁶M. Gmitra, S. Konschuh, C. Ertler, C. Ambrosch-Draxl, and J. Fabian, *Phys. Rev. B* **80**, 235431 (2009).
- ³⁷H. Min, B. Sahu, S. K. Banerjee, and A. H. MacDonald, *Phys. Rev. B* **75**, 155115 (2007).
- ³⁸G. Giuliani and G. Vignale, *Quantum Theory of the Electron Liquid* (Cambridge University Press, Cambridge, 2005).
- ³⁹M. J. Lighthill, *Introduction to Fourier Analysis and Generalized Functions* (Cambridge University Press, Cambridge, 1958).
- ⁴⁰T. Ando, *J. Phys. Soc. Jpn.* **75**, 074716 (2006).
- ⁴¹G. Gómez-Santos and T. Stauber, *Phys. Rev. Lett.* **106**, 045504 (2011).
- ⁴²R. Sensarma, E. H. Hwang, and S. Das Sarma, *Phys. Rev. B* **82**, 195428 (2010).
- ⁴³S. Gangadharaiah, A. M. Farid, and E. G. Mishchenko, *Phys. Rev. Lett.* **100**, 166802 (2008).
- ⁴⁴X.-F. Wang and T. Chakraborty, *Phys. Rev. B* **75**, 041404(R) (2007).
- ⁴⁵I. S. Gradshteyn and I. M. Ryzhik, *Table of Integrals, Series, and Products* (Academic Press, London, 2000).
- ⁴⁶D. Xiao, G.-B. Liu, W. Feng, X. Xu, and W. Yao, *Phys. Rev. Lett.* **108**, 196802 (2012).